An Electrochemical in Situ Surface-Enhanced Raman Spectroscopic Study of Carbon Monoxide Chemisorption at a Gold Core-Platinum Shell Nanoparticle Electrode with a Flow Cell

ARTICLE *in* THE JOURNAL OF PHYSICAL CHEMISTRY C · SEPTEMBER 2009

Impact Factor: 4.77 · DOI: 10.1021/jp906697b · Source: OAI

An Electrochemical in Situ Surface-Enhanced Raman Spectroscopic Study of Carbon Monoxide Chemisorption at a Gold Core−Platinum Shell Nanoparticle Electrode with a Flow Cell

Pu Zhang,[†] Yan-Xia Chen,*[,†] Jun Cai,[†] Sang-Zi Liang,[†] Jian-Feng Li,[‡] An Wang,[‡] Bin Ren,[‡] and Zhong-Qun Tian[‡]

Hefei National Laboratory for Physical Sciences at Microscale and Department of Chemical Physics, University of Science and Technology of China, Hefei, 230026, China, and State Key Laboratory of Physical Chemistry of Solid Surfaces and Department of Chemistry, College of Chemistry and Chemical Engineering, Xiamen University, Xiamen, 361005, China

Received: July 15, 2009; Revised Manuscript Received: August 12, 2009

The adsorption behavior of a CO adlayer at a Au core−Pt shell (Au@Pt) nanoparticle electrode as a function of CO coverage, partial pressure, and electrolyte composition is examined by electrochemical in situ surface-enhanced Raman spectroscopy (SERS) combined with a thin layer flow cell, which allows time-resolved spectro-electrochemical measurements upon sudden exchange of the electrolyte under potential control. We find (i) a clear decrease (increase) in the Pt−CO_L (C−O_L) peak frequency and an increase of both bands' intensities with CO_{ad} coverage; (ii) a slight increase in the Pt−CO_L and decrease in the C−O_L stretching frequencies and an increase in both intensities of the CO_{ad}-saturated layer when switching from CO-saturated to CO-free solution; (iii) a clear decrease (up to 50%) of intensities of all of the Pt−CO and C−O bands and the SERS background during the solution switch from H_2SO_4 or NaOH to Na_2SO_4; (iv) a slightly higher C−O_L (lower Pt−CO_L) peak frequency in H_2SO_4 than that in Na_2SO_4 and NaOH. The contributions of different factors such as SERS enhancement, Pt−CO binding strength, CO molecular orientation, and dynamic dipole−dipole coupling interactions among the CO_{ad} molecules to the SERS spectral behavior are discussed on the basis of the complementary information of both Pt−CO and C−O stretching vibrations.

1. Introduction

At platinum based electrocatalysts on the anode of low temperature solid polymer fuel cells, CO is a common poisoning adsorbate or reaction intermediate coming either from the hydrogen feed gas with a trace amount of CO as impurities or from the dissociative adsorption of small organic molecules.[1−6] A fundamental understanding of the nature and energy of CO surface bonding on Pt as well as of how these properties are affected by its chemical, electrostatic, and geometric environments will be of great help to alleviate the CO poisoning problem in the fuel cell anode. To this end, extensive studies on the adsorption/oxidation of CO at Pt based electrodes have been carried out using various in situ vibrational spectroscopies such as electrochemical infrared absorption spectroscopy (EC-IRAS) and sum frequency generation (SFG), since these methods are proved to be the most powerful techniques in probing the nature and configuration of surface adsorbate.[7−9]

Systematic vibrational spectroscopic studies reveal that, on the Pt surface, (i) CO prefers a multiply bonded configuration toward negative potential;[10] (ii) C−O stretching frequency (ν_{C-O}) increases linearly with electrode potential (the so-called Stark effect);[10] (iii) ν_{C-O} increases with CO_{ad} surface coverage;[11,12] (iv) ν_{C-O} increases and C−O band intensities decrease with the increase in CO partial pressure when the CO_{ad} layer remains saturated at corresponding pressure.[13] Despite these achievements, due to the alternation of the spectral behavior of the C−O stretching band by the strong dipole−dipole coupling effects between the nearby CO_{ad} molecules, there is no direct correlation between CO adsorption energy and C−O stretching frequency or between the band intensity of C−O stretching vibration and CO_{ad} surface coverage. On the other hand, the dipole−dipole coupling effects for the metal−CO vibration are much weaker (100 times smaller) than those for the C−O vibration.[14] Thus, the complementary information of metal−CO stretching will be of great help to infer parameters such as binding energies, molecular orientation, and surface coverage of CO on the metal surface.

So far, vibrational spectroscopic results on intermolecular Pt−CO stretching are sparse. In the electrochemical environment, due to the limited transparencies of the IR window (normally >800 cm^{-1}) as well as the strong absorption in the far-infrared region of water which presents as the commonly used solvent in such studies, the information on Pt−CO stretching cannot be provided by EC-IRAS. Even under ultra-high vacuum (UHV) conditions, there are only a few studies by infrared and electron energy loss spectroscopy (EELS) observing the stretching band of Pt−CO at Pt(111).[14−19] In contrast, surface-enhanced Raman spectroscopy (SERS) can obtain vibrational information in a wide spectral window (5−4000 cm^{-1}) and need not use the spectral-difference method to remove solution-phase interferences. However, few in situ electrochemical studies have been carried out on CO adsorption on Pt substrate, since SERS studies on pure roughened Pt electrodes are largely limited by the poor surface sensitivity. To surmount this problem, Weaver and Tian et al. developed an "intensity borrowing strategy" with skin layer Pt deposited

* To whom correspondence should be addressed. E-mail: yachen@ustc.edu.cn.
[†] University of Science and Technology of China.
[‡] Xiamen University.

10.1021/jp906697b CCC: $40.75
Published on Web 09/14/2009

onto a roughened Au electrode or Au nanoparticles, where the adsorbates at the Pt layers win great enhancement in their Raman signal due to the long-range effect of the enormous electromagnetic enhancement created by the highly SERS-active Au substrate.[20−23] By this, they have observed well-defined Pt−CO stretching in addition to C−O stretching vibration of the saturated CO adlayer at Pt skin layers deposited on a roughened Au electrode or Au nanoparticles.[21,24] Though the methodology has been well proved, so far, there have been no systematic studies on the SERS behavior of CO at a Pt electrode.

With this strategy, we have carried out detailed studies on the effects of CO surface coverage, partial pressure, electrolyte composition (solution pH), and electrode potential on the vibrational properties of Pt−CO and C−O stretching of the CO_{ad} layer at a Au core−Pt shell nanoparticle electrode using electrochemical in situ SERS combined with a thin layer flow cell. The nanoparticles with a 55 nm Au core coated with a 0.7 nm thick Pt shell (denoted as 55 nm Au@0.7 nm Pt hereafter) were chosen as the electrode substrate, which can provide more than 100 times higher intensity in Raman signal than that from an electrochemically roughened Pt electrode. To make sure that the Au substrate was completely covered by the Pt overlayer and hence to avoid possible interference from the CO adsorbed at the neighboring Au, a thickness of the Pt shell of 0.7 nm (ca. 2 monolayers) rather than 0.35 nm was chosen.

The paper is organized as follows: After the description of the general experimental procedure, the SERS behavior as a function of the CO adlayer coverage and partial pressure at constant potentials will be discussed. Then, we present the results on the SERS behavior of CO upon the changes of electrolyte composition (and pH) at constant potential and CO partial pressure. The effect of electrode potential on the SERS behavior will be discussed elsewhere.[25] The contributions of different factors such as SERS enhancement, Pt−CO binding strength, CO molecular orientation, and dynamic dipole−dipole coupling interactions among the CO_{ad} molecules to the SERS spectral behavior are discussed on the basis of the complementary information of both Pt−CO and C−O stretching vibrations.

2. Experimental Section

$HAuCl_4$ (A. R.), H_2PtCl_6 (A. R.), sodium citrate (A. R.), ascorbic acid (A. R.), Na_2SO_4 (A. R.), H_2SO_4 (G. R.), and NaOH (G. R.) were purchased from Shanghai Reagent Corporation, China. Millipore Milli-Q water (18.2 MΩ cm) was used throughout the study. Before SERS measurements, all of the electrolyte solutions were deaerated by continuous N_2 (4N, from Linde Gas China) purging. CO-saturated solution was achieved by prepurging the supporting electrolyte with pure CO (99.9%, from Linde Gas China) for 15 min in the electrolyte reservoir and with continuous purging during the experiments.

55 nm Au@0.7 nm Pt nanoparticles were prepared by coating a thin layer (0.7 nm) of Pt over 55 nm Au nanoparticles following the report by Tian's group.[21] In brief, after synthesizing the Au nanoparticles with a diameter of ca. 55 nm by reducing $AuCl_4^-$ using sodium citrate, 30 mL of sol containing 55 nm Au seeds was mixed with 0.76 mL of 1 mM H_2PtCl_6 and heated to 80 °C for several minutes. Then, 0.4 mL of 10 mM ascorbic acid was slowly dropped into the above mixtures through a syringe controlled by a step motor under vigorous stirring. The mixtures were further stirred for about 20 min to ensure complete reduction of H_2PtCl_6. After that, the 55 nm Au@0.7 nm Pt sol was centrifuged three times to remove excess reactants. Then, the remaining sol (5 μL) was cast on a smooth Pt electrode (diameter ca. 1.5 mm) and dried in a desiccator,

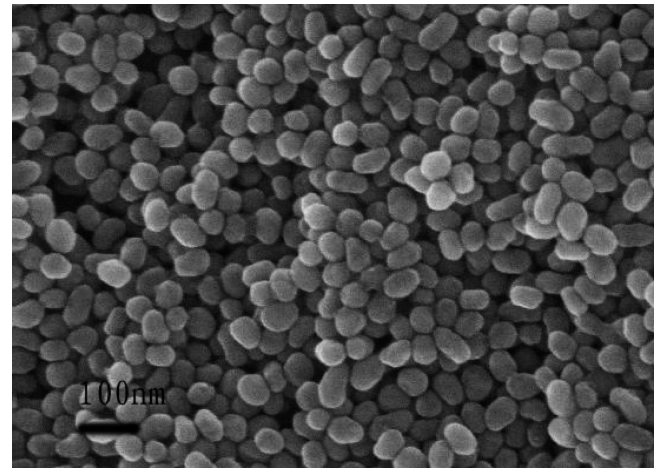

Figure 1. SEM image of 55 nm Au@0.7 nm Pt core−shell nanoparticles assembled on a polycrystalline electrode.

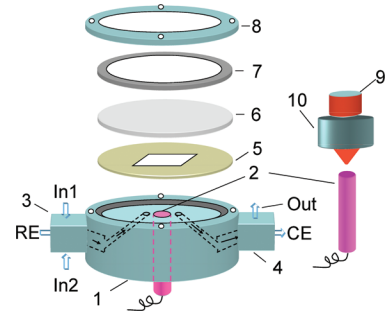

Figure 2. Schematic illustration of the spectro-electrochemical flow cell for Raman measurements: (1) Kel-F cell body; (2) working electrode; (3) four-way connector for inlet capillaries and RE; (4) three-way connector for outlet capillaries and CE; (5) PTFE membrane spacer; (6) quartz optical window; (7) silicone rubber O-ring; (8) stainless steel cover; (9) incident He−Ne laser beam; (10) microscope objective.

and this procedure was repeated three times to ensure the Pt electrode was completely covered by Au@Pt nanoparticles. The nanoparticles display ellipsoidal shape with uniform size distribution, as demonstrated in the scanning electron microscope (SEM) image in Figure 1.

Electrochemical measurements were conducted using a CHI631B electrochemical workstation (CH Instruments, Shanghai, China). The design of the electrochemical flow cell for Raman spectroscopic study was largely based on the knowledge of the spectro-electrochemical flow cell for EC-IRAS studies with the attenuated total reflection configuration by Chen et al.[26] Figure 2 shows the sketch of the spectro-electrochemical flow cell, which consisted of a circular Kel-F (poly(chlorotrifluoroethylene)) cell body (1) with a cylindrical hole in the middle for mounting the working electrode (WE, (2)) and openings for inlet and outlet capillaries on two sides. The left-hand capillary was connected to a four-way connector (3) with two ports connecting to inlet capillaries and one to the reference electrode (RE) and the right-hand capillary connected to the three-way connector (4) which connected both the outlet capillary and the counter electrode (CE). A flat quartz window (6) was mounted into the cell with a thin film PTFE spacer (5) pressed against the cell body, the thickness of the spacer can be adjusted between 0.1 and 1 mm, which determined the thickness of the electrolyte layer above the working electrode. A thin Au foil (thickness 50 μm) was used as the CE, and a saturated calomel electrode (SCE) was used as the reference electrode (RE). A silicone rubber O-ring (7) was pressed against the quartz window

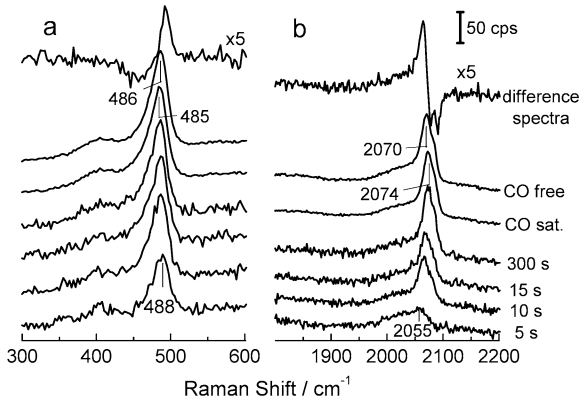

Figure 3. SER spectra of Pt−CO (a) and C−O (b) from adsorbed CO on 55 nm Au@0.7 nm Pt/Pt as a function of time upon switching to CO-saturated 0.5 M H_2SO_4 and then switching back to CO-free 0.5 M H_2SO_4 at a constant potential of 0.06 V. The spectra were taken with 5 s per spectrum. The spectra of the saturated CO_{ad} layer in CO-saturated and in CO-free solution after being averaged with 20 spectra recorded under each condition and the differences between these two cases are given in the top.

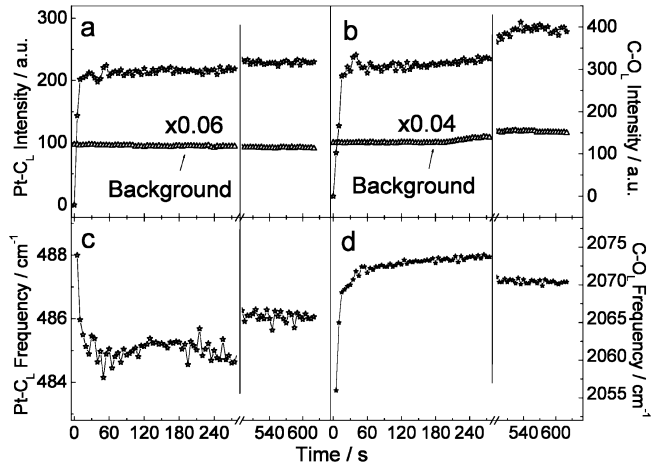

Figure 4. Raman band intensity (a,b) and peak frequencies (c,d) of Pt−CO (a,c) and C−O (b,d) from adsorbed CO on 55 nm Au@0.7 nm Pt/Pt as a function of time upon switching to CO-saturated 0.5 M H_2SO_4 and then back to CO-free 0.5 M H_2SO_4 at a constant potential of 0.06 V. Other conditions are the same as in Figure 3. The corresponding SERS background changes are also shown as triangles in parts a and b.

by a stainless steel circle (8) to fix the whole cell. The electrolyte flow through the cell can be switched between different electrolyte reservoirs, and the flow rate was controlled by hydraulic pressure in the reservoirs. In this experiment, the flow rate was 50 μL/s. All measurements were performed at ambient temperature (25 ± 3 °C). All potentials are reported with respect to normal hydrogen electrode (NHE) in this paper.

SERS measurements were carried out with a confocal microprobe Raman system (LabRam I from Dilor, France) using an air−cooled CCD and a He−Ne laser operating at 632.8 nm. About 10 mW of laser power was delivered to the working electrode surface (beam diameter ca. 2 μm) through the microscope attachment based on an Olympus BX40 system using a long working length (8 mm) ×50 objective. An 1800 g/mm grating was used to provide a spectral resolution of 2 cm^{-1} to discern the small changes in peak frequencies (a resolution of about 1 cm^{-1} can be achieved when the grating is fixed).

3. Results and Discussion

3.1. The Effects of CO Coverage and Partial Pressure on SERS of CO at Constant Potential. ***3.1.1. Coverage-Dependent SERS Behavior at Au@Pt.*** The time-resolved coverage-dependent SERS measurements were carried out as follows: in N_2 deaerated 0.5 M H_2SO_4 solution, the potential of the 55 nm Au@0.7 nm Pt nanoparticle electrode was held at a constant value of 0.06 V; then, the solution was changed to CO-saturated 0.5 M H_2SO_4 for 300 s and then switched back to CO-free supporting electrolyte. Upon the electrolyte switch, SER spectra in the range from 250 to 1050 cm^{-1} (covering the Pt−CO stretching vibration) were recorded sequentially with a time resolution of 5 s per spectrum. After oxidative removal of CO_{ad} at 0.85 V and completely cleaning the cell by flushing with N_2 deaerated 0.5 M H_2SO_4, the same experiment was repeated to record the spectra in the range from 1600 to 2250 cm^{-1} (covering the C−O stretching vibration).

Representative sets of SERS spectra of Pt−CO and C−O vibrations recorded during the CO adsorption are shown in Figure 3. It is evident that, upon exposing the 55 nm Au@0.7 nm Pt nanoparticle film electrode to the CO-saturated solution, two bands at ca. 2055 and 488 cm^{-1} with a small shoulder at ca. 410 cm^{-1} appear. The higher frequency band at 2055 cm^{-1} is assigned to intramolecular vibration of linearly bonded CO (C−O_L).[8,11,15,27] On the basis of previous work in UHV[14,15,17−19] and the pioneering electrochemical in situ SERS studies on Pt overlayers on Au,[22,24] the lower frequency band located at ca. 488 cm^{-1} is attributed to the metal−adsorbate stretching vibration of linearly bonded CO (Pt−CO_L) and the small shoulder at ca. 410 cm^{-1} is assigned to intermolecular vibration of multiply bonded CO (Pt−CO_M). It should be mentioned that in one earlier study by EELS the band at ca. 410 cm^{-1} was assigned to the frustrated rotation of CO at Pt.[28] The SERS signal in the region from 1750 to 1900 cm^{-1} where intramolcular vibration of multiply bonded CO (C−O_M) is expected to appear is quite weak; however, in neutral and basic solutions and at relatively negative potential region, we observe stronger bands from C−O_M (~1830 cm^{-1}) stretching which is well-correlated with the band at ~410 cm^{-1} (see Figure 8). This further confirms that the assignment of the band at ca. 410 cm^{-1} to Pt−CO_M is reasonable. In addition, the lack of the characteristic C−O stretching vibration from CO adsorbed at the Au surface (above 2100 cm^{-1}) confirms that the 0.7 nm Pt overlayers on the Au core are pinhole free. The much smaller C−O_M and Pt−CO_M band intensties than those of C−O_L and Pt−CO_L reveals that the latter is energetically more stable at the electrode potential examined in the present study. Since Pt−CO_M and C−O_M bands in acid solution are very weak, the discussion in this section will mainly focus on C−O_L and Pt−CO_L stretching.

Figure 4 gives the changes of integral band intensities and peak frequencies of both Pt−CO_L and C−O_L vibrations as a function of time upon electrolyte exchange derived from the obtained Raman spectra. With the increasing exposure time of the 55 nm Au@0.7 nm Pt nanoparticle electrode to CO-saturated solution, the peak frequency of Pt−CO_L (ν_{Pt-CO_L}) decreases and reaches a constant value of 485 cm^{-1} and the C−O_L stretching frequency (ν_{C-O_L}) increases steadily up to 2074 cm^{-1} after ca. 30 s. In addition to the frequency changes, the integral band intensities of both Pt−CO_L and C−O_L stretching increase with the time for CO exposure and reach a maximum value at ca. 30 s. Such spectral changes suggest that the surface coverage of CO increases with the exposure of the clean electrode to CO-saturated solution and reaches saturation in ca. 30 s. It should be noted that, with the same flow cell setup, it takes ca. 10 s to saturate the smooth polycrystalline Pt electrode. This is ex-

plained by the fact that the nanoparticle film is relatively thick and densely compacted and there are lots of tiny pores among these nanoparticles, so it takes a longer time for CO molecules to penetrate through the pores before approaching the nanoparticles in the sublayers.

Factors which may cause frequency shift upon the changes in CO_{ad} surface coverage are (i) variation in the adsorption sites such as from terrace to steps or vice versa, (ii) dynamic dipole−dipole coupling effects between CO_{ad} molecules, and (iii) chemical effects due to charge transfer between substrate and adsorbates. In the following, we will discuss these factors point by point.

Obviously, a large amount of defects and steps exist on a Au@Pt nanoparticle film electrode, which are distinct from the terrace sites at a single crystalline or smooth polycrystalline Pt electrode. At low temperatures in UHV, it is commonly accepted that once the CO molecules find a site (no matter terrace or defect sites) at the Pt surface it sticks there, since the thermal excitation energy (e.g., ~1.2 kJ/mol at 100 K) is much smaller than the activation energy for its surface diffusion (ca. 25 kJ/mol).[29] After the surface with low CO_{ad} surface coverage is annealed at higher temperatures and then goes back to lower temperatures again, CO previously adsorbed at terrace sites has been found to shift to defect sites with characteristic lower $C-O_L$ peak frequencies.[30] In contrast, the present experiments were done at room temperature, where the thermal excitation ($3/2RT$ ~3.7 kJ/mol, where $T = 298$ K) is high enough to allow the CO_{ad} molecules to diffuse at a certain rate along the Pt surfaces. Thus, it can be considered that the adsorbed CO molecules are uniformly distributed over the Pt surface (i.e., the terrace, step, and defect sites are statistically occupied). This means that the contribution from preferential occupation of CO at defects or steps to the coverage-dependent peak frequency changes is negligible.

On the other hand, with the increase in CO_{ad} surface coverage, the increase in the dynamic dipole−dipole coupling effects among the adsorbed CO_{ad} molecules will cause a blue-shift in the $C-O_L$ peak frequencies according to dynamic dipole−dipole coupling theory.[31,32] It should be noted that dipole−dipole coupling effects for Pt−CO stretching are nearly 2 orders smaller than those for C−O stretching;[14] thus, the contribution of dipole−dipole coupling to the Pt−CO vibration is negligible. Hence, we conclude that chemical effects dominate the red-shift in Pt−CO peak frequency toward higher CO_{ad} surface coverage. Such chemical effects may come either from the alternation of 5σ (CO) → sp (Pt) donation or d (Pt) → $2\pi^*$(CO) back-donation or from the superimposition of both as a result of the enhanced CO−CO repulsion at higher CO_{ad} surface coverage. The red-shift of ν_{Pt-CO_L} proves the weakening of the Pt−CO bond. On the other hand, both the reduction of d (Pt) → $2\pi^*$ (CO) back-donation and the increase in the dipole−dipole coupling effects with the increase in CO_{ad} coverage will cause a blue-shift of ν_{C-O_L}. Unfortunately, due to band broadening caused by surface heterogeneity as a result of the surface roughness associated with such nanoparticle electrodes, it is not possible to use the isotope dilution method to quantify the contribution from chemical effects and dipole−dipole coupling effects to the coverage-dependent Pt−CO and C−O peak frequency changes.

In addition to the dielectric screening, competition among neighboring adsorbate molecules for the surface charge density involved in d (Pt) → $2\pi^*$ (CO) back-donation is often proposed as the origin for the chemical effects which induce the blue-shift of C−O stretching frequency.[33] Here, we would like to emphasize that this assumption may hold for the cases under UHV conditions, but it will not be applicable for the cases in an electrochemical environment at constant potential. In an electrochemical environment, the charge density of the electrode surface will remain constant when the electrode potential and other conditions are held unchanged, i.e., any net charge transfer due to 5σ (CO) → sp (Pt) donation and d (Pt) → $2\pi^*$(CO) back-donation between the electrode and adsorbates will be fast equilibrated by the feedback circuit of the potentiostat. Thus, in principle, at constant potential, every CO_{ad} molecule at identical surface sites can receive the same amount of charge as what the first adsorbed CO molecule does, provided that the charges can be freely transferred. However, at higher CO_{ad} surface coverage, the extent of charge transfer between metal and adsorbates may vary due to the dielectric screening. Further theoretical investigations or novel experimental strategies are necessary to get a deeper understanding for such a system.

3.1.2. The Effect of CO Partial Pressure on the SERS Behavior of the Saturated CO_{ad} Layer. Another interesting phenomenon observed in the present study is that when the electrolyte is switched back to CO-free solution after the surface is fully saturated with CO, ν_{Pt-CO_L} increases from 485 to 486 cm^{-1} and ν_{C-O_L} decreases from 2074 to 2070 cm^{-1}, while the intensities of the $C-O_L$ and $Pt-CO_L$ bands increase about 30 and 6%, respectively (Figures 3 and 4). It should be noted that 1 cm^{-1} spectral change is just on the scale of the spectral resolution of the Raman spectrometer. In order to make sure this spectral change is not an artifact and to improve signal/noise ratio, we have averaged over 20 spectra recorded in CO-saturated or CO-free H_2SO_4 solution (see Figure 3). To better identify the changes of the SERS bands of the saturated CO adlayer with and without saturated CO in the solution, we subtracted the spectrum taken in CO-free solution by that taken in CO-saturated solution. The difference spectra obtained are displayed in the top of Figure 3 (note that the difference spectra have been amplified 5 times in order to clearly see the spectral difference at the same scale of those without any treatment; a table which summarizes the delicate spectral changes upon the changes in CO partial pressure or in electrolyte composition can be found in the Supporting Information). The bipolar shape of such difference spectra clearly demonstrates that both $Pt-CO_L$ and $C-O_L$ stretching frequencies of the saturated CO adlayer changes with the CO partial pressure.

Furthermore, it was found that such spectral changes are quite reproducible no matter when repeating the experiments with the same electrode after the oxidation of preadsorbed CO at 0.85 V or making a new electrode with the same procedure. Furthermore, the same phenomenon has been observed on 55 nm Au@1.4 nm Pt core−shell nanoparticles with ca. 4 MLs of Pt, which suggests that the lattice mismatch (between the Pt shell and Au substrate) is not the critical issue for the partial-pressure-dependent Raman spectral behavior of the saturated CO adlayer. On the other hand, the spectral changes in the $C-O_L$ band of the saturated CO adlayer, i.e., the increase in the $C-O_L$ band intensity and decrease in the $C-O_L$ peak frequency with CO partial pressure are quite similar to the recent results on CO adsorption at a rough polycrystalline Pt film electrode under otherwise identical conditions measured by infrared spectroscopic study.[13,25] Furthermore, it is noticed that, in the similar study by EC-IRAS, a clear decrease in $C-O_M$ band intensity is also observed when switching to CO-free solution after the surface is fully saturated with CO in CO-saturated solution,[25] while, in the present study by SERS, the $C-O_M$ band is barely discernible. Anyway, the intimate

similarity for the spectral changes of the CO_L band suggests that such a partial-pressure-dependent spectral behavior should represent a general phenomenon which reflects the adlayer structure or coverage changes with CO partial pressure in the solution. Since the factors which determine the SERS intensity differ greatly from those of infrared spectroscopy, in the present paper, we will only focus on discussing the SERS behavior of the CO adsorbates. A detailed discussion on the comparison of the SERS and infrared spectral behavior of CO adsorption will be given elsewhere.[25]

From a recent study using scanning tunneling microscopy (STM), it was found that the coverage of the saturated CO adlayer at the Pt/gas interface increases with the concentration of CO in the solution.[34] According to either the Langmuir or Temkin adsorption isotherm, it is expected that at the Pt electrode/electrolyte interface the equilibrial CO_{ad} surface coverage should be slightly higher in CO-saturated solution than that in CO-free solution under otherwise identical conditions. Unfortunately, at the moment, we could not accurately figure out the small coverage decrease when switching from CO-saturated solution to CO-free solution because the CO_{ad} surface coverage obtained by CV has an error as much as 5%. The slightly higher packing density of CO in CO-saturated solution may lift all of the adsorbed CO molecules to a weaker adsorbed state with a slightly longer Pt−CO distance due to the stronger CO−CO repulsion. Since the dipole−dipole coupling effects of the Pt−CO stretching are negligible,[14] the slight peak frequency increase for $Pt-CO_L$ (from 485 to 486 cm^{-1}) of the saturated CO adlayer following the removal of CO in the solution can be rationalized by the small change in chemical effects associated with the charge transfer between the Pt electrode and CO_{ad} molecules (i.e., 5σ (CO) → sp (Pt) donation and d (Pt) → $2\pi^*$(CO%) back-donation), which reveals the increase in the Pt−CO bonding strength when lowering the CO surface coverage (partial pressure). However, a net decrease in $C-O_L$ stretching frequency from 2074 to 2070 cm^{-1} is attributed to the decrease in the dipole−dipole coupling interaction in addition to an increase in d-$2\pi^*$ back-donation.

Then, what are the origins for the ~6 and ~30% lower band intensities for $Pt-CO_L$ and $C-O_L$ stretching vibrations of the CO adlayer in CO-saturated solution compared to the case in CO-free solution, although the CO_{ad} surface coverage in the former case is slightly higher than that in the latter? Factors which may induce the changes of the intensities of $Pt-CO_L$ and $C-O_L$ stretching of the saturated CO adlayer with CO partial pressure are (i) SERS enhancement; (ii) site conversion, e.g., from CO_M to CO_L with a decrease in CO partial pressure; (iii) dipole−dipole coupling effects; and (iv) tilting of the CO molecular axis.

Generally, two major factors have been proposed for SERS enhancement mechanisms, electromagnetic enhancement and chemical enhancement.[35] Electromagnetic enhancement mainly comes from geometrically defined suface plasmon resonances, and chemical enhancement correlates to the charge transfer between the adsorbed molecule and the surface. On the basis of the facts that (i) the structure of the nanoparticle electrode does not change during the experiments, since the same experiments can be well reproduced with the same electrode, and (ii) there is no clear change in the SERS background signal upon switching to CO-free solution (see Figure 4; note that the background values are calculated by subtracting the corresponding peak areas and normalized to fit into the page), we conclude that the changes in the electromagnetic enhancement and chemical enhancement factors for SERS are negligible. Since the band intensities of both $C-O_M$ and $Pt-CO_M$ are too weak to judge their spectral change, its contribution to the overall band intensity changes should be small.

When taking the dynamic dipole coupling effects into account, the Raman intensity of surface adsorbate can be expressed as shown below:[36]

$$I_{\text{Raman}} \propto \frac{[(\partial\alpha_A/\partial Q)_0 Q \cos\phi]^2}{\{1 + [\alpha_{A0} + (\partial\alpha_A/\partial Q)_0 Q]\tilde{U}(0)\}^4} \quad (1)$$

where $\tilde{U}(0)$ is the coupling constant that describes the intensity of dipole−dipole coupling among the molecules in the adlayer.[31,32] Obviously, this constant depends on the geometric arrangement of the molecule. α_A is the polarizability of one single adsorbed CO molecule on metal. ϕ is the tilting angle of the CO molecular axis to the surface normal. Q is the normal coordinate of Pt−C or C−O stretching. The subscript "0" represents the value in the equilibrium position. According to Eq. (1), the Raman intensity changes linearly with $(\cos\phi)^2$ and $(\tilde{U}(0))^{-4}$. From Eq. (1), it is easily seen that the vibrational mode with its polarizability perpendicular to the local surface normal gives the highest SERS intensity, as determined by the surface selection rule of SERS.

The tilting of the Pt−C and C−O molecular axis of chemically adsorbed CO molecules to the surface normal by the continuous bombarding of the surface with CO from the solution phase or by the repulsion from instantaneous physically adsorbed CO molecules is well confirmed in previous studies under UHV conditions.[37,38] For $Pt-CO_L$ stretching, since the dynamic dipole coupling effects can be negligible, the 6% lower $Pt-CO_L$ band intensity in CO-saturated solution is preliminarily attributed to the decrease of cos ϕ, while the 30% lower band intensity of $C-O_L$ stretching in CO-saturated solution than that in CO-free solution is mainly attributed to the higher dielectric screening in the former case as a result of dynamic dipole coupling effects when the CO_{ad} surface coverage is slightly higher (the increase of $\tilde{U}(0)$).

At last, we would like to comment that it is generally believed that the IR results can be taken as an average of the signal from all of the sampled Pt surface, while the SERS signal mainly comes from the hot spots. Since in the present SERS study we obtain similar partial-pressure-dependent spectral behavior as that observed in rough Pt film by ATR-FTIRS,[25,39] we believe the SERS signal (although mainly from hotspots) can be representative of the structural change of the adlayer on all the nanoparticle surfaces. This will be further discussed in detail elsewhere.[25] Despite the complexities associated with the peak frequencies of C−O stretching vibration and the band intensities of both vibrations, the Pt−CO peak frequency can always be taken as a direct measure for the strength of Pt−CO bonding. In fact, the continuous decrease in Pt−CO peak frequency with an increase in CO_{ad} surface coverage correctly reflects the weakening of Pt−CO bonding toward higher coverages as a result of the increase in repulsion among adsorbed CO_{ad} molecules at higher CO_{ad} surface coverages which is in good agreement with literature reports.[40]

3.2. SERS Behavior of the Saturated CO_{ad} Layer at the Pt Surface upon the Electrolyte Switch. In order to check whether the electrolyte in the double layer, i.e., the chemical nature of the ions, the composition, and the pH of the solution, affects the adsorption/desorption behavior of CO as well as the structure of the saturated CO adlayer, we have monitored the Raman spectral behavior upon changing the electrolyte while fixing the electrode potential as well as the CO partial pressure (the

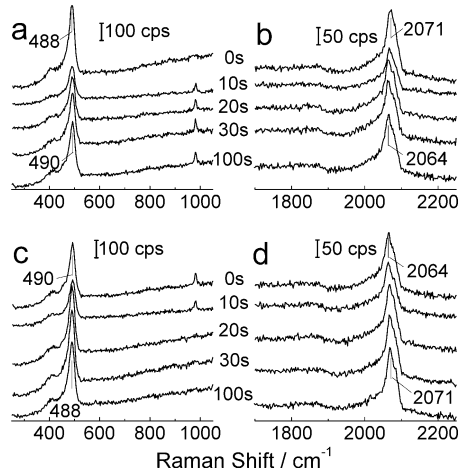

Figure 5. SER spectra of Pt−CO (a,c) and C−O (b,d) from adsorbed CO on 55 nm Au@0.7 nm Pt/Pt at −0.1 V as a function of time upon forward switch from CO-saturated H_2SO_4 to CO-saturated Na_2SO_4 solution (a,b) and the corresponding backward solution switch (c,d). The spectra were taken with 10 s per spectrum.

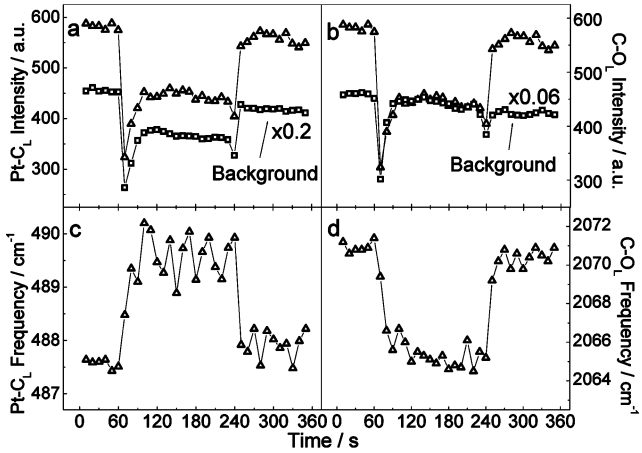

Figure 6. Raman band intensity (a,b) and peak frequencies (c,d) of Pt−CO_L (a,c) and C−O_L (b,d) from adsorbed CO on 55 nm Au@0.7 nm Pt/Pt (triangles) as a function of time upon switching between CO-saturated 0.5 M H_2SO_4 and Na_2SO_4 solutions at −0.1 V. The corresponding SERS background changes are also shown as squares in parts a and b. The other conditions are the same as those in Figure 5.

solutions always saturated with CO). For the SERS measurement when switching between 0.5 M H_2SO_4 and 0.5 M Na_2SO_4 (or 0.5 M Na_2SO_4 and 0.5 M NaOH), the electrode potential was held at −0.1 (or −0.55 V) in order to avoid the possible interference from the oxidation of CO in both solutions as well as from HER to the measurements.

3.2.1. Spectral Changes of the Saturated CO_{ad} Layer upon the Switch between H_2SO_4 and Na_2SO_4. Sequences of Raman spectra recorded at −0.1 V with a time resolution of 10 s per spectrum when switching from 0.5 M H_2SO_4 to 0.5 M Na_2SO_4 and then back to 0.5 M H_2SO_4 are shown in Figure 5. To better illustrate the spectral changes upon the electrolyte switch, the changes of frequency and band intensity as a function of time upon the electrolyte switch are plotted and shown in Figure 6. From Figures 5 and 6, two bands with peak frequencies at 2071 (C−O_L) and 1850 cm^{-1} (C−O_M) and a broadband with two discernible peaks at 411 (Pt−CO_M) and 490 cm^{-1} (Pt−CO_L) stretching vibrations are seen. Within the first 10 s of the switch from 0.5 M H_2SO_4 to 0.5 M Na_2SO_4, a clear decrease in the intensities of all the C−$O_{L,M}$ and Pt−$CO_{L,M}$ bands (up to 50%)

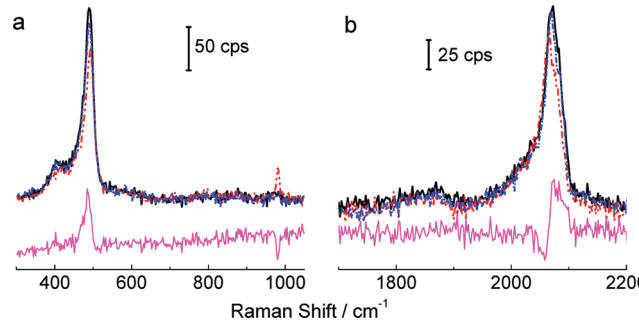

Figure 7. SER spectra of Pt−CO (a) and C−O (b) from adsorbed CO on 55 nm Au@0.7 nm Pt/Pt in CO-saturated 0.5 M H_2SO_4 and 0.5 M Na_2SO_4 solutions at −0.1 V. Solid line, in 0.5 M H_2SO_4 before solution switch; dash−dotted line, after switching back to 0.5 M H_2SO_4; dotted line, in 0.5 M Na_2SO_4; bottom line: the difference of spectra recorded in 0.5 M H_2SO_4 and 0.5 M Na_2SO_4 solutions.

is observed, accompanied with the appearance of a small band at ca. 982 cm^{-1} from the symmetric vibration of SO_4^{2-} in Na_2SO_4 whose band intensity reaches a maximum in ca. 10−20 s after the solution switch.[41,42] We find that this peak frequency does not change with electrode potential, which suggests that sulfate anions are located in the solution phase rather than in the chemically adsorbed state. All of the CO_{ad} related band intensities increase from 10 to 40 s after the solution switch; then, afterwards, they reach constant values. Compared with the Raman spectra recorded in 0.5 M H_2SO_4 before the solution switch, the steady-state intensities of all of the bands in 0.5 M Na_2SO_4 are ca. 25% smaller (see Figures 5 and 6). On the other hand, a decrease in C−O_L streching frequency from 2071 to 2064 cm^{-1} and an increase in Pt−CO_L frequency from 488 to 490 cm^{-1} are noticed within the first 20 s after the solution switch. Afterward, the changes in all of the peak frequencies are neglibile. It is noticed that the changes in the peak frequencies lag behind the band intensity changes for ca. 10 s. Furthermore, no obvious change in the band shape is observed during the solution switch. Within the first 10 s of switching from 0.5 M Na_2SO_4 back to 0.5 M H_2SO_4, all of the band intensities also decrease, as is similar to the case when switching from 0.5 M H_2SO_4 to 0.5 M Na_2SO_4, but the drop only amounts to about 10% of the total band intensity. The band intensities increase in the next 40 s until the steady-state values are reached, which is accompanied by the decrease in the ν_{Pt-CO_L} value of ca. 2 cm^{-1} and an increase of 7 cm^{-1} with ν_{C-O_L}. Again, the peak frequency changes lag ca. 10 s behind the abrupt intensity change. The steady-state peak frequencies and band intensities after switching back to 0.5 M H_2SO_4 are nearly the same as the values obtained in 0.5 M H_2SO_4 prior to the electrolyte change, as shown in Figure 7.

To eliminate any possible artifacts from the experiments, we have repeated the experiments very carefully and found that such phenomena are quite reproducible, which reveals that the origins which cause such spectral changes are reversible upon such electrolyte exchange. Judging from the appearance and disappearance of the sulfate band upon the solution switch, we found that it takes ca. 10−20 s for the complete exchange of electrolyte solution using our present flow cell setup. This time domain is just within the period when the SERS signal of CO is lower than that before and after the complete solution switch, suggesting that this abrupt band intensity drop must be introduced by the solution switch.

3.2.2. Spectral Changes of the Saturated CO_{ad} Layer upon the Switch between NaOH and Na_2SO_4. Time-resolved SER spectra recorded upon switching between 0.5 M NaOH and 0.5

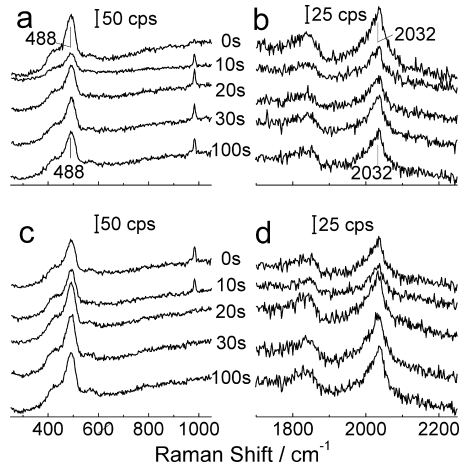

Figure 8. SER spectra of Pt−CO (a,c) and C−O (b,d) from adsorbed CO on 55 nm Au@0.7 nm Pt/Pt at −0.55 V as a function of time upon switching between CO-saturated 0.5 M NaOH and Na_2SO_4 solutions: from NaOH to Na_2SO_4 (a,b) and from Na_2SO_4 to NaOH (c,d). The spectra were taken with 10 s per spectrum.

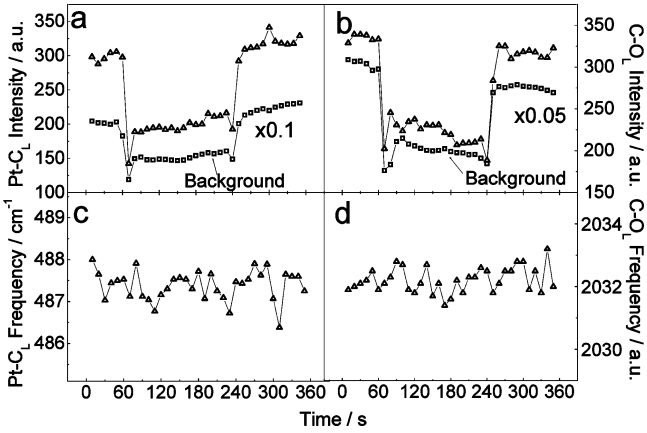

Figure 9. Raman band intensity (a,d) and peak frequencies (c,d) of Pt−CO_L (a,c) and C−O_L (b,d) from adsorbed CO on 55 nm Au@0.7 nm Pt/Pt as a function of time upon switching between CO-saturated 0.5 M NaOH and Na_2SO_4 solutions at −0.55 V. The corresponding SERS background changes are also shown as squares in parts a and b. The other conditions are the same as those in Figure 8.

M Na_2SO_4 at −0.55 V (Figures 8 and 9) also exhibits an initial decrease in all of the C−$O_{L,M}$ band intensities (up to 50%) accompanied with the appearance of the SO_4^{2-} band at 982 cm^{-1} within the first 10 s after the solution switch. From 10 to 20 s, all CO_{ad} related band intensities increase; then, afterwards, the steady-state values are reached. It is noticed that in 0.5 M Na_2SO_4 the integral band intensities under steady-state conditions are ca. 35% lower than those in 0.5 M NaOH. When switching back from 0.5 M Na_2SO_4 to 0.5 M NaOH, an initial decrease of all of the CO related bands has also been noticed within the first 10 s; then, afterwards, the band intensities increase and reach steady-state values in ca. 30 s. Again, the band shape remains largely unchanged during the solution switch.

In contrast to the case when the switch occurs between 0.5 M H_2SO_4 and 0.5 M Na_2SO_4, no changes in Pt−$CO_{L,M}$ and C−$O_{L,M}$ peak frequencies are detected throughout the solution switch process (Figures 8−10). Furthermore, during the solution switch between 0.5 M Na_2SO_4 and 0.5 M NaOH, a small band at ca. 572 cm^{-1} is observed, which is assigned to Pt−OH stretching.[43] However, this band is only observed during the solution switch where the electrolyte composition in the double

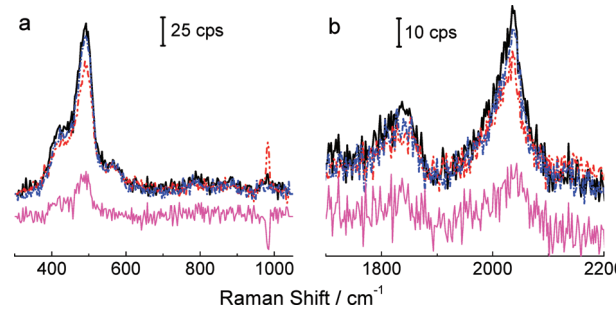

Figure 10. SER spectra of Pt−CO (a) and C−O (b) from adsorbed CO on 55 nm Au@0.7 nm Pt/Pt between CO-saturated 0.5 M NaOH and Na_2SO_4 solutions at −0.55 V. Solid line, before the solution switch in 0.5 M NaOH; dash−dotted line, after switching back to 0.5 M NaOH; dotted line, in 0.5 M Na_2SO_4; bottom line, the difference of spectra recorded in 0.5 M NaOH and 0.5 M Na_2SO_4 solutions.

layer is under vigorous changes (Figure 8). By careful inspection of the spectral sequence upon the solution switch, we found that the band of Pt−OH stretching blinks with time. This is probably due to the fact that OH^- anions are in a dynamic adsorption−desorption process upon the change in the double layer structure. By comparing Figures 5−10, the spectral behavior upon switching from acid to neutral solution and from alkaline to neutral solution and the corresponding backward switch are quite similar and reversible. Furthermore, no changes in the band intensity ratios, i.e., I_{Pt-CO_L}/I_{Pt-CO_M} and I_{C-O_L}/I_{C-O_M}, are discerned, suggesting that under the present experimental conditions the effect of the electrolyte composition on the CO site occupation is negligible.

3.2.3. Origins of Peak Frequency Changes upon the Electrolyte Switch. What are the origins for the changes of peak frequencies of both Pt−CO and C−O stretching vibrations upon switching the electrolyte between H_2SO_4 and Na_2SO_4, while in the cases when switching between NaOH and Na_2SO_4 no changes in peak frequencies has been discerned? In 0.5 M H_2SO_4 and at −0.1 V, the coadsorption of H atoms can be easily inferred from the occurring hydrogen evolution reaction (HER) process which most probably takes place in the free spaces which are not occupied by CO_{ad} molecules (e.g., CO island edges), as confirmed by the small cathodic current observed under such conditions. It should be mentioned that, due to the small surface coverage as well as the short lifetime (involved in the dynamic HER process), the Pt−H vibration is not observed in the present SERS measurements.

The coadsorbed H atoms with CO have the following features: (i) the amount of such adsorbed H atoms is small; (ii) they locate at the edges of the CO islands; (iii) the bond length of Pt−H is much shorter than that of Pt−CO, especially when H atoms are adsorbed at the hollow sites; (iii) at most sites of the Pt surface, the binding energy of CO molecules is higher than that of H atoms; (iv) H atoms can only be adsorbed at the statisticial surface sites among the CO adlayer to which CO molecules are not accessbile due to steric hindrance.[44−47] Hence, the replacement of CO or abrupt change of CO adlayer structure by the pre- or postadsorbed H atoms is less likely, but a small lateral shift of CO molecules from their previous positions may take place when switching between the states with and without coadsorbed H atoms.[46−48]

With this model, in the existence of coadsorbed H atoms in 0.5 M H_2SO_4, a slight compression of CO_{ad} molecules may take place which may shift a small fraction of the CO molecules located at near atop to exact atop position; this will cause a 7 cm^{-1} blueshift in the C−O_L stretching frequency and 2 cm^{-1}

decrease in the $Pt-CO_L$ stretching frequency. As already described above, the peak frequency changes lag ca. 10 s behind that of the band intensity changes, which suggests that the origins for the peak frequency and band intensity changes are differnent; this will be further discussed in the following section. In the case when switching between NaOH and Na_2SO_4, since the coverage of coadsorbed OH^- anions will be much less, the change of CO adlayer structure will be neglibile; as a result, no changes in peak frequencies have been discerned.

3.2.4. Origins of SERS Band Intensity Changes upon the Electrolyte Switch. The most intriguing phenomenon observed in the present study is the up to 50% band intensity changes upon switching the electrolyte. Possible origins which may cause such spectral changes upon switching the electrolyte are (i) coverage or structure of CO adlayer, (ii) dynamic dipole−dipole coupling interactions among the adsorbed CO_{ad} molecules, (iii) refractive index of the electrolyte, and (iv) SERS enhancement factors. In the following, we will discuss these points one by one.

The higher saturated CO_{ad} surface coverage in Na_2SO_4 than that in H_2SO_4 or NaOH is less likely, since this should lead to a higher $C-O_L$ peak frequency as already discussed in section 3.1; however, this is opposite to what has been observed in the present study. On the other hand, since the binding strength for CO at the Pt electrode is much stronger than that of sulfate or hydrated sodium cations and no anodic current was observed under the present conditions, an abrupt decrease in CO_{ad} surface coverage by CO_{ad} desorption or CO_{ad} oxidation upon electrolyte switch is less likely. Furthermore, since similar band intensity changes (up to 50%) are found for both solution switches between Na_2SO_4 and H_2SO_4 or Na_2SO_4 and NaOH, the origin for the band intensity change by coadsorbed H atoms can be excluded. The dipole−dipole coupling effects can also be excluded on the basis of the fact that, though the dipole−dipole coupling effects of Pt−CO vibration are far smaller than those of C−O vibration, the intensity changes of Pt−CO and C−O vibration bands mount to the same extent during the solution swich procedure.

From a similar experiment using a silicon wafer as the working electrode, we find that the band intensity of the first-order Si−Si vibration at 520.6 cm^{-1} as well as the corresponding background signal are almost constant during the solution switch process between 0.5 M H_2SO_4 and 0.5 M Na_2SO_4. This reveals that such spectral changes do not originate from the shift of the focus plane of the incident laser beam induced by the alternation of the refractive index of the electrolyte, which is also surpported by the small differences in the refractive index of the electrolytes such as Na_2SO_4, H_2SO_4, and NaOH. All of these facts point to the fact that the changes in the SERS band intensities of Pt−CO and C−O stretching vibrations most probably result from the changes of SERS enhancement factors during the solution switch.

On the basis of the fact that the band intensity changes (e.g., shown in Figures 7 and 10) are relatively reversible throughout the electrolyte switch (except little irreversible decrease in the overall band intensity with time), the effect from the change in the geometry structure of the electrode surface can be negligible. Thus, the contribution from the corresponding change in electromagnetic enhancement to up to 50% band intensity can be excluded. Instead, the band intensity change should mainly result from the change in chemical enhancement factor for SERS. There are three well-known mechanisms for the chemical enhancement of SERS: (i) chemical-bonding enhancement, (ii) surface-complex enhancement, and (iii) photon-induced charge-transfer enhancement. Obviously, the first two mechanisms can be easily excluded, while the third one is also less likely based on the following reasons: If this mechanism operates, the band intensity changes must originate from the changes in the difference between the energy levels of the highest occupied molecular orbital (HOMO) or lowest unoccupied molecular orbital (LUMO) of the adsorbates and the Fermi level of the metal substrate. Any such changes should be sensitively reflected in the changes in C−O and Pt−CO stretching frequencies, but as discussed above, the changes in the peak frequencies and the band shape are rather small and the peak frequency does not change simultaneously with the band intensity changes at all.

To further figure out the chemical origin for the band intensity changes, we examined carefully the change in the integral intensities of background signal from 430 to 520 cm^{-1} and from 1920 to 2110 cm^{-1} upon the electrolyte switch and plotted the curves in Figures 6 and 9 (squares, note that the background values are calculated by subtracting corresponding peak areas and normalized to fit into the page). Obviously, the background intensity−time dependency follows approximately the temporal evolution in the intensities of $Pt-CO_L$ and $C-O_L$ bands, suggesting that factors which affect the background signal and the SERS intensities of $Pt-CO_L$ and $C-O_L$ bands are probably of the same origin. The background signal may originate from processes such as luminescence or electronic Raman scattering of the substrate, which are closely related to the first layer effect in SERS. Domke et al. found that the background signal correlates with the number of adsorbates in a tip-enhanced Raman spectroscopy (TERS) study.[49] However, our present data are not enough to correlate such changes simply to the changes of the number of CO_{ad} molecules, since there is no simple correlation between the band intensity (background intensity) and peak frequencies. Further investigations are underway to obtain a deep understanding of the exact origin of such effects.

4. Conclusions

Taking the advantage of a fast and convenient switch in the electrolyte composition by a thin layer flow cell, we have examined the effects of CO surface coverage, CO partial pressure, and electrolyte composition (solution pH) on the vibrational properties of Pt−CO and C−O stretching of the CO adlayer at 55 nm Au@0.7 nm Pt core−shell nanoparticle electrodes using electrochemical in situ SERS.

With an increase in CO_{ad} surface coverage, a clear decrease (increase) in the $Pt-CO_L$ ($C-O_L$) peak frequency together with an increase of all of the band intensities are observed. The chemical effects are found to be responsible for the frequency change of the $Pt-CO_L$ stretching band, and both the chemical and the dipole−dipole coupling effects within adsorbed CO molecules are the main causes for the frequency change of $C-O_L$. The monotonic decrease in $Pt-CO_L$ peak frequency with the increase in the surface coverage of the CO_{ad} layer unambiguously reveals the decrease in the CO adsorption strength at the Pt surface with coverage. With the solution switch from CO-saturated H_2SO_4 to CO-free H_2SO_4, the intensities of $Pt-CO_L$ and $C-O_L$ increase 6 and 30%, respectively, together with a slight change in the peak frequency. The intensity change of $Pt-CO_L$ is mainly attributed to the CO axis orientation tilting in the case under continuous CO bombarding, while the dipole–dipole coupling effects, chemical effects, and the CO axis orientation tilting are responsible for the intensity and frequency changes of the $C-O_L$ stretching vibration.

The SERS spectra recorded upon changes in the electrolyte between H_2SO_4, Na_2SO_4, and NaOH at constant potentials reveal

a substantial change (up to 50%) in the band intensities of Pt−CO and C−O stretching vibrations. In addition, the $C-O_L$ ($Pt-CO_L$) peak frequency is ca. 7 cm^{-1} higher (2 cm^{-1} lower) in H_2SO_4 than that in Na_2SO_4, while no differences in the peak frequencies have been discerned when switching between Na_2SO_4 and NaOH. A small lateral shift of CO_{ad} from atop edges to exactly atop positions upon the coadsorption of H atoms in H_2SO_4 has been proposed to explain such a frequency change, while the band intensity changes are identified to be due to the changes in the chemical enhancement factor upon the electrolyte switch; however, the exact origins for the change in chemical enhancement factor still need to be clarified.

These results clearly demonstrate that the SER spectral behavior of CO changes very sensitively with the electrolyte composition, CO partial pressure, CO_{ad} surface orientation, and CO_{ad} surface coverages. In addition, the complementary information of both Pt−CO and C−O stretching vibrations obtained by SERS can help us to correctly understand the SERS mechanism as well as to correctly deduce information such as adlayer structure, binding energy, and molecule orientation. The results from the present study greatly improved our understanding on the nature and energy of CO surface bonding on roughed Pt (especially on Pt nanoparticles applied in fuel cells) as well as of how these properties are affected by its chemical, electrostatic, and geometric environments.

Finally, we would like to emphasize that it will not be possible to obtain the results presented in this study without using an electrochemical flow cell. The general potential of electrochemical in situ Raman spectroscopic studies under continuous flow conditions with well-defined mass transport to/from the electrode extends far beyond the result given in the present paper, e.g., it can be exploited for kinetic and mechanistic spectro-electrochemical studies for sensors, electroanalysis, as well as electrocatalytic reactions involving all kinds of reactants including dissolved gases or other dilute reactants. Furthermore, this technique allows: (i) transient, time-resolved spectro-electrochemical measurements upon sudden exchange of the electrolyte under potential control; (ii) spectro-electrochemical adsorption/stripping measurements of nonvolatile species; and (iii) modification of electrode surfaces by chemical or electrochemical adsorption/deposition in the flow cell prior to the actual measurements, which opens the way for a direct evaluation of different electrocatalysts.

Acknowledgment. This work was supported by 100 Talents' Program of The Chinese Academy of Science, grants of the National Natural Science Foundation of China (NSFC) (Project No. 20773116), State Key Laboratory of Physical Chemistry of Solid Surfaces of Xiamen University (Project No. 200706), and the 973 program (Project No. 2010CB923302) from the Ministry of Science and Technology (MOST) of China.

Supporting Information Available: The derivation of formula for Raman intensity/frequency and a table summarizing band intensity/frequency changes under different experimental conditions. This material is available free of charge via the Internet at http://pubs.acs.org.

References and Notes

(1) Parsons, R.; VanderNoot, T. *J. Electroanal. Chem.* **1988**, *257*, 9.
(2) Beden, B.; Leger, J. M.; Lamy, C. In *Modern Aspects of Electrochemistry*; White, R. E.; Bockris, J. O. M.; Conway, B. E., Eds.; Plenum Press: New York, 1992.
(3) Jarvi, T. D.; Stuve, E. M. In *Electrocatalysis*; Lipkovski, J.; Ross, P. N., Eds.; Wiley-VCH: New York, 1998.
(4) Sun, S.-G. In *Electrocatalysis*; Lipkowski, J., Ross, P. N., Eds.; Wiley-VCH: New York, 1998; p 243.
(5) Markovic, N. M.; Ross, P. N. *Surf. Sci. Rep.* **2002**, *45*, 121.
(6) Korzeniewski, C. In *Advances in Electrochemical Science and Engineering*; Alkire, R. C.; Kolb, D. M.; Lipkowski, J.; Ross, P. N., Eds.; Wiley-VCH: New York, 2006.
(7) Peremans, A.; Tadjeddine, A.; Zheng, W. Q.; Le Rille, A.; Guyot-Sionnest, P.; Thiry, P. A. *Surf. Sci.* **1996**, *368*, 384.
(8) Iwasita, T.; Nart, F. C. *Prog. Surf. Sci.* **1997**, *55*, 271.
(9) Baldelli, S.; Markovic, N.; Ross, P.; Shen, Y. R.; Somorjai, G. *Abs. Pap. Am. Chem. Soc.* **2000**, *219*, U522.
(10) Roth, J. D.; Chang, S. C.; Weaver, M. J. *J. Electroanal. Chem.* **1990**, *288*, 285.
(11) Chang, S.-C.; Weaver, M. J. *J. Chem. Phys.* **1990**, *92*, 4582.
(12) Chen, Y. X.; Heinen, M.; Jusys, Z.; Behm, R. J. *J. Phys. Chem. C* **2007**, *111*, 435.
(13) Heinen, M.; Chen, Y. X.; Jusys, Z.; Behm, R. J. *ChemPhysChem* **2007**, *8*, 2484.
(14) Persson, B. N. J.; Ryberg, R. *Phys. Rev. B* **1989**, *40*, 10273.
(15) Baro, A. M.; Ibach, H. *J. Chem. Phys.* **1979**, *71*, 4812.
(16) Severson, M. W.; Russell, A.; Campbell, D.; Russell, J. W. *Langmuir* **1987**, *3*, 202.
(17) Tobin, R. G.; Richards, P. L. *Surf. Sci.* **1987**, *179*, 387.
(18) Hoge, D.; Tühaus, M.; Schweizer, E.; Bradshaw, A. M. *Chem. Phys. Lett.* **1988**, *151*, 230.
(19) Baily, C. J.; Surman, M.; Russell, A. E. *Surf. Sci.* **2003**, *523*, 111.
(20) Tian, Z. Q.; Ren, B.; Li, J. F.; Yang, Z. L. *Chem. Commun.* **2007**, 3514.
(21) Li, J. F.; Yang, Z. L.; Ren, B.; Liu, G. K.; Fang, P. P.; Jiang, Y. X.; Wu, D. Y.; Tian, Z. Q. *Langmuir* **2006**, *22*, 10372.
(22) Mrozek, M. F.; Xie, Y.; Weaver, M. *J. Anal. Chem.* **2001**, *73*, 5953.
(23) Zou, S. Z.; Weaver, M. *J. Anal. Chem.* **1998**, *70*, 2387.
(24) Zou, S. Z.; Weaver, M. J. *J. Phys. Chem.* **1996**, *100*, 4237.
(25) Chen, Y. X.; Behm, R. J. In preparation.
(26) Chen, Y. X.; Heinen, M.; Jusys, Z.; Behm, R. B. *Angew. Chem., Int. Ed. Engl.* **2006**, *45*, 981.
(27) Chang, S.-C.; Weaver, M. J. *Surf. Sci.* **1990**, *238*, 142.
(28) Bare, S. R.; Hofmann, P.; King, D. A. *Surf. Sci.* **1984**, *144*, 347.
(29) Kobayashi, T.; Babu, P. K.; Gancs, L.; Chung, J. H.; Oldfield, E.; Wieckowski, A. *J. Am. Chem. Soc.* **2005**, *127*, 14164.
(30) Xu, J. Z.; Yates, J. T. *J. Chem. Phys.* **1993**, *99*, 725.
(31) Persson, B. N. J.; Ryberg, R. *Phys. Rev. B* **1981**, *24*, 6954.
(32) Severson, M. W.; Stuhlmann, C.; Villegas, I.; Weaver, M. J. *J. Chem. Phys.* **1995**, *103*, 9832.
(33) Weaver, M. J. *Appl. Surf. Sci.* **1993**, *67*, 147.
(34) Davies, J. C.; Nielsen, R. M.; Thomsen, L. B.; Chorkendorff, I.; Logadottir, A.; Lodziana, Z.; Norskov, J. K.; Li, W. X.; Hammer, B.; Longwitz, S. R.; Schnadt, J.; Vestergaard, E. K.; Vang, R. T.; Besenbacher, F. *Fuel Cells* **2004**, *4*, 309.
(35) Moskovits, M. *J. Raman Spectrosc.* **2005**, *36*, 485.
(36) See the Supporting Information for equations on SERS.
(37) Persson, B. N. J.; Tushaus, M.; Bradshaw, A. M. *J. Chem. Phys.* **1990**, *92*, 5034.
(38) Tushaus, M.; Berndt, W.; Conrad, H.; Bradshaw, A. M.; Persson, B. *Appl. Phys. A* **1990**, *51*, 91.
(39) Heinen, M.; Chen, Y. X.; Jusys, Z.; Behm, R. J. *Electrochim. Acta* **2007**, *53*, 1279.
(40) Ertl, G.; Neumann, M.; Streit, K. M. *Surf. Sci.* **1977**, *64*, 393.
(41) Brown, G. M.; Hope, G. A. *J. Electroanal. Chem.* **1995**, *382*, 179.
(42) Li, X.; Heryadi, D.; Gewirth, A. A. *Langmuir* **2005**, *21*, 9251.
(43) Zhang, Y.; Gao, X. P.; Weaver, M. J. *J. Phys. Chem.* **1993**, *97*, 8656.
(44) Lenz, K.; Poelsema, B.; Bernasek, S. L.; Comsa, G. *Surf. Sci.* **1987**, *189−190*, 431.
(45) Bernasek, S. L.; Lenz, K.; Poelsema, B.; Comsa, G. *Surf. Sci.* **1987**, *183*, L319.
(46) Hoge, D.; Tühaus, M.; Bradshaw, A. M. *Surf. Sci.* **1988**, *207*, L935.
(47) Roeterdink, W. G.; Bonn, M.; Olsen, R. A. *Chem. Phys. Lett.* **2005**, *412*, 482.
(48) Barth, J. V. *Surf. Sci. Rep.* **2000**, *40*, 75.
(49) Domke, K. F.; Zhang, D.; Pettinger, B. *J. Am. Chem. Soc.* **2006**, *128*, 14721.

JP906697B